Electronic Supplementary Information for

Kirkendall effect-assisted synthesis of hollow MoS_2 nanospheres with interlayer expansion for improved magnesium diffusion kinetics and durability

Ruqi Cai,†[a] Han Qin,†[a] Xianbo Yu,*[a] Feng Yan,*[b] Xiangming Wang,[a] Yang Zhao,[a] Baoning Wang,[a] Xitian Zhang*[a]

[a]Key Laboratory for Photonic and Electronic Bandgap Materials, Ministry of Education, School of Physics and Electronic Engineering, Harbin Normal University, Harbin 150025, China

[b]Key Laboratory of In-Fiber Integrated Optics, Ministry of Education, College of Physics and Optoelectronic Engineering, Harbin Engineering University, Harbin 150001, China

† Ruqi Cai and Han Qin contributed equally to this work.

*Corresponding author.

E-mail address: ge_yuxianbo@126.com (X. Yu); yanfeng@hrbeu.edu.cn (F. Yan); xtzhang@hrbnu.edu.cn (X. Zhang)

Experimental Section

Chemicals. All the chemicals were not further purified. Glycerol ($C_3H_8O_3$, AR, 99%), isopropanol (C_3H_8O, AR, 99.7%), and sodium sulfide hydrate nine ($Na_2S·9H_2O$) were purchased from Aladdin Biochemical Science and Technology Co. LTD (Shanghai, China).

Synthesis of MoGs. Molybdenum-glycerate spheres (MoGs) were synthesized by solvent pyrolysis. Firstly, 200 mg of molybdenum pentachloride ($MoCl_5$) and 19 mL

of glycerol were dispersed into 50 mL of isopropanol. The mixed solution was stirred for about 20 min until $MoCl_5$ was completely dissolved and mixed to obtain a homogeneous mixed solution. The homogeneous mixed solution was then placed into a Teflon-lined autoclave and kept at 200°C for 3 h. After the solution was cooled down to room temperature, it was washed and centrifuged with water and absolute ethanol at a speed of 8000 r for 5 min. Finally, it was placed into an oven and kept at 60°C for 12 h and dried to a dark brown powder sample.

Synthesis of EH-MoS_2, EH-MoS_2-3, and EH-MoS_2-10. Firstly, 120 mg of MoGs was dispersed with 300 mg of $Na_2S{\cdot}9H_2O$ into 60 mL of absolute ethanol, and the solution was stirred for 45 min until it was homogeneously dispersed. The above mixed solution was then transferred into a Teflon-lined autoclave and kept in an oven at 180°C for 6 h. After the solution was cooled to room temperature, it was washed and centrifuged with water and absolute ethanol. After dried in an oven at 40°C for 12 h, the EH-MoS_2 was obtained. Similarly, EH-MoS_2-3 and EH-MoS_2-10 were prepared under the same conditions as preparation of EH-MoS_2 except the reaction time of 3 h and 10 h at 180°C in a Teflon-lined autoclave.

Synthesis of FH-MoS_2. To show the disadvantages of 1T phase, FH-MoS_2 (with 2H phase of MoS_2) was prepared by annealing EH-MoS_2 at 500°C for 2 h under argon and hydrogen mixture (H_2/Ar) gas.

Materials characterization.

The morphology and structure of all the catalysts were observed by the X-ray diffractometer (XRD, PANalytical X′Pert PRO), scanning electron microscope (SEM, Hitachi SU8010) and transmission electron microscope (TEM, Tecnai G^2 F30). The specific surface area of the sample and its adsorption properties were detected by specific surface area testing (BET, ASAP 2020). The chemical compositions and the vibrational rotational energy level were detected by the X-ray photoelectron spectroscopy (XPS, AXIS SUPRA+) and Raman spectroscopy (Raman, LabRAMHR800).

Electrochemical Measurements.

All the electrochemical measurements were performed by a two-electrode

configuration, and the CR2025-type coin cells were assembled in an argon-filled glove box with moisture and oxygen level <0.1 ppm with as-prepared materials as cathodes, polished Mg plates as anodes, and microporous membrane (Celgard 2400) as separators. The cathodes were prepared by mixing active material, with polyvinylidene difluoride (PVDF), and acetylene black at a weight ratio of 8:1:1 to form a homogeneous slurry and pasting onto the carbon fiber paper with the loading of 1.0 mg cm^{-2}. All-phenyl complex (APC) electrolyte for MIBs was prepared as follows: 2.133 g of aluminium chloride ($AlCl_3$) was slowly added into 24 mL of anhydrous tetrahydrofuran (THF) solution and vigorous stirring for 12 h, and then 16 mL of phenyl magnesium chloride (MgPhCl) solution in THF was added dropwise to form the APC electrolyte under vigorous stirring for another 12 h. EIS measurements were obtained in a frequency range from 0.1 Hz to 100 kHz.

Galvanostatic intermittent titration technique (GITT) was carried out using a multichannel battery test system. The batteries were measured for 5 min discharge and 15 min relaxing time at the current density of 20 mA g^{-1}. The diffusion coefficient can be calculated by Fick' second law:

$$D = \frac{4}{\pi\tau}\left(\frac{m_b V_m}{M_b S}\right)^2\left(\frac{\Delta E_s}{\Delta E_t}\right)^2$$

where τ is the time of current pulse. V_m, m_b, and M_b represent molar volume, the mass, and molar mass of materials, respectively. S is the contact area of electrode/electrolyte. ΔE_s and ΔE_t are the steady-state potential change by the current pulse and potential change during the constant current, which are eliminated with the *IR* drop.

Computational methods.

The density functional theory (DFT) calculations were performed using the projector augmented wave (PAW). The generalized gradient approximation in the form of the Perdew–Burke–Ernzerhof functional with a cut-off energy of 500 eV to calculate exchange-correlation energy. The energy convergence was 10^{-5} eV and the geometry optimizations forces used the convergence criterion of 0.01 eV $Å^{-1}$. The transition states were localized using the climbing image nudged elastic band method (CI-NEB) as implemented in the Transition State Tools for VASP module. A bilayer model has been

used for MoS_2 in this work with 4 × 4 × 1 supercell with a vacuum larger than 10 Å, sampled with 3 × 3 × 1 Monkhorst-Pack grid; the interlayer distances were fixed to 6.25 and 7.27 Å.

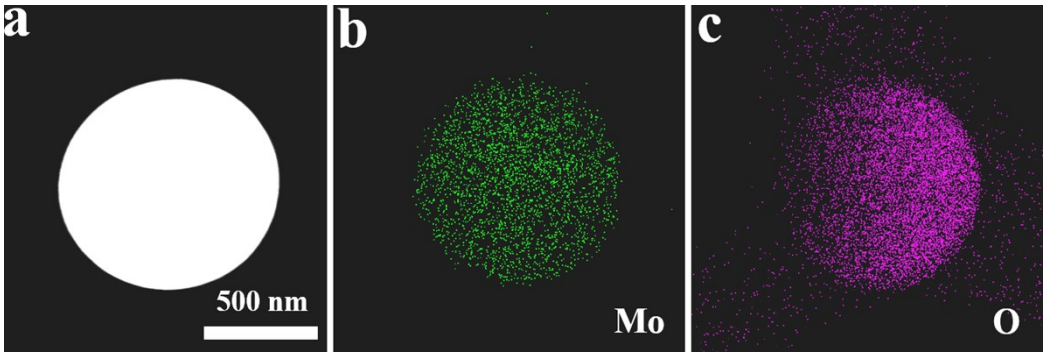

Fig. S1 (a-c) EDS element mapping images of the MoG nanosphere.

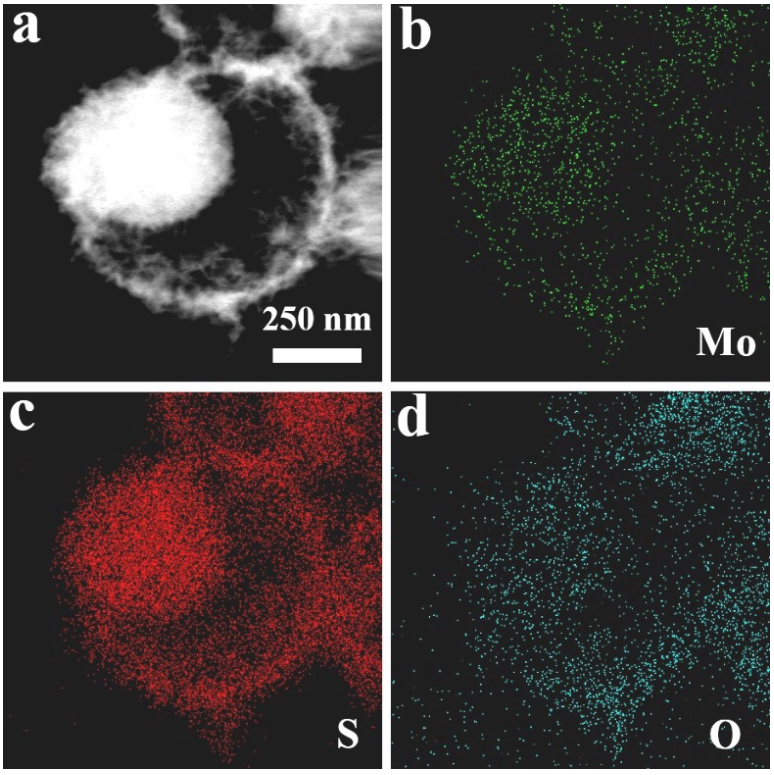

Fig. S2 (a-d) EDS element mapping images of the EH-MoS_2-3 nanosphere.

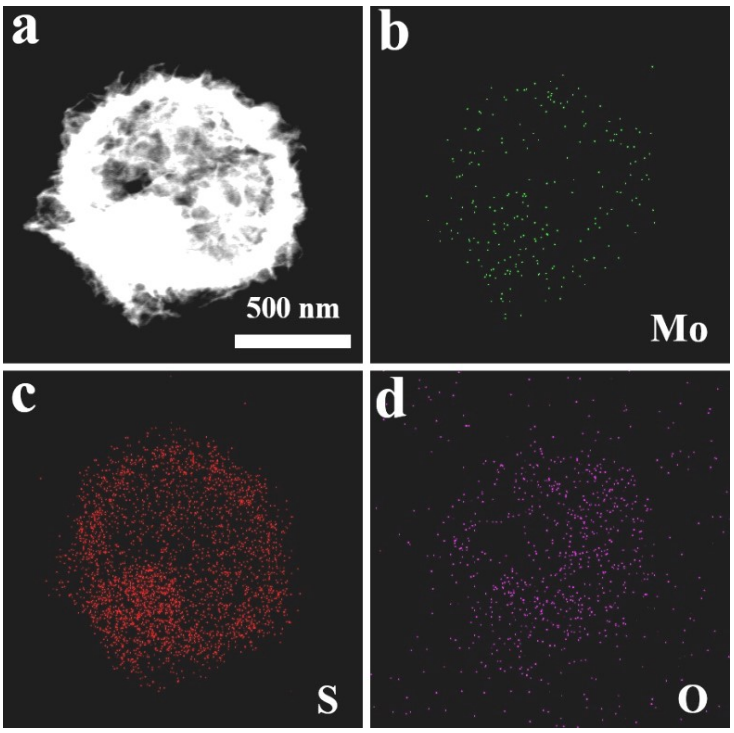

Fig. S3 (a-d) EDS element mapping images of the EH-MoS_2-5 nanosphere.

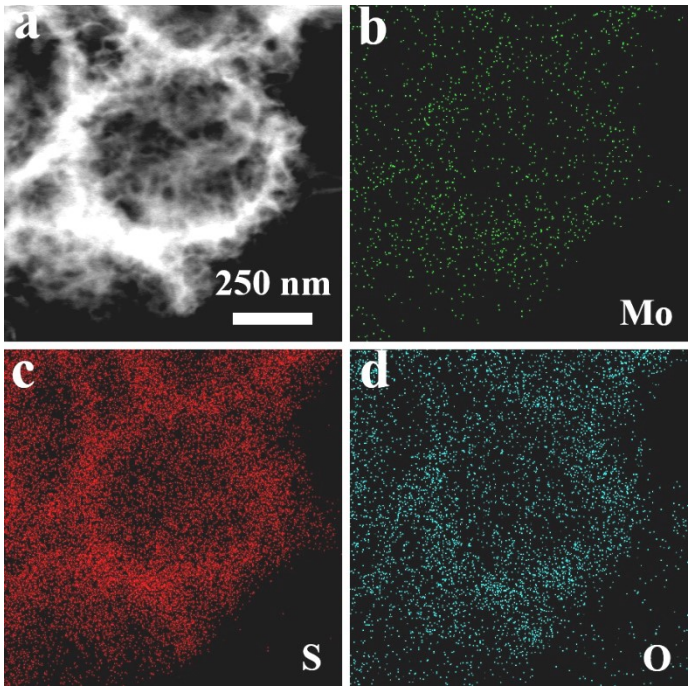

Fig. S4 (a-d) EDS element mapping images of the EH-MoS_2 nanosphere.

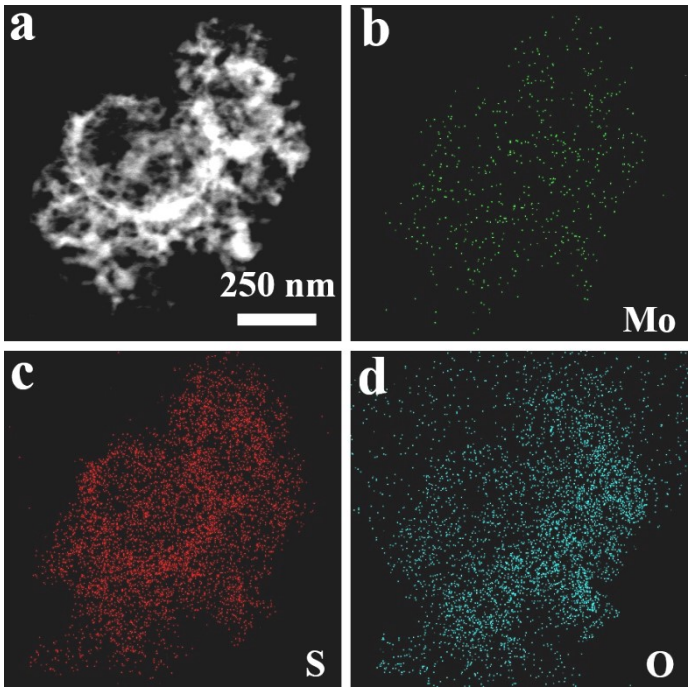

Fig.S5 (a-d) EDS element mapping images of an individual EH-MoS_2-10 nanosphere.

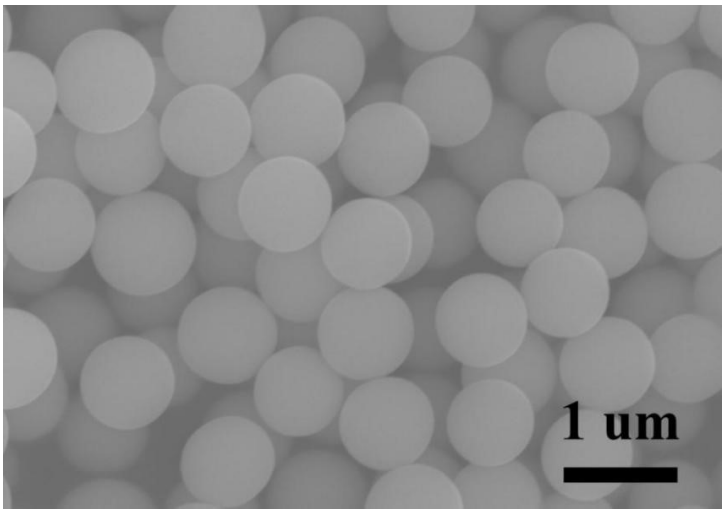

Fig. S6 SEM image of MoGs.

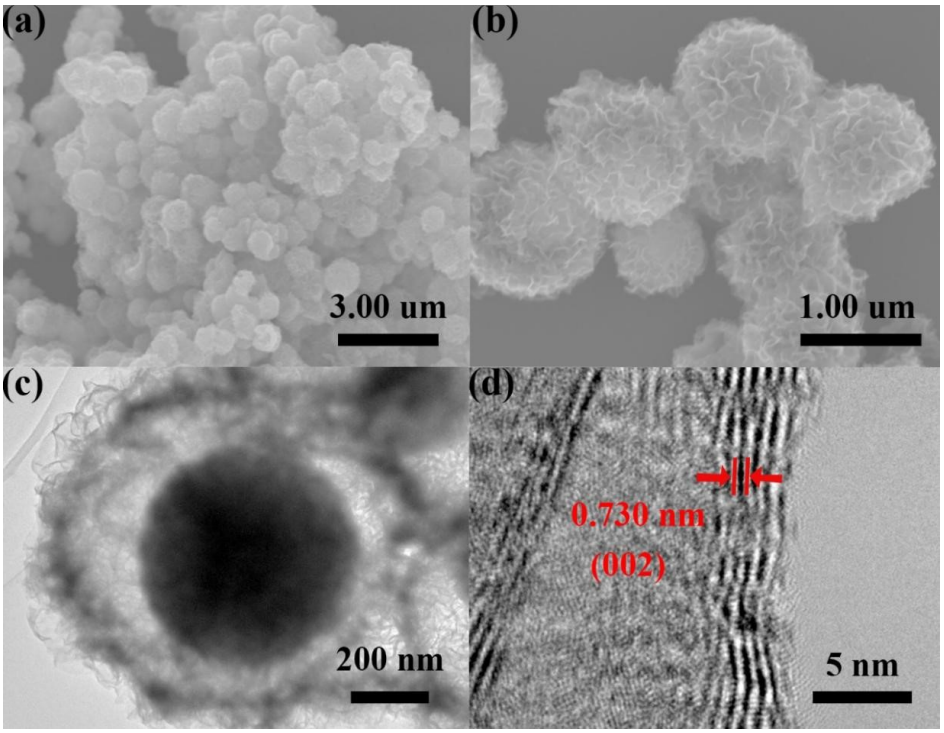

Fig. S7 (a,b) SEM, (c) TEM, and (d) HRTEM images of EH-MoS_2-3.

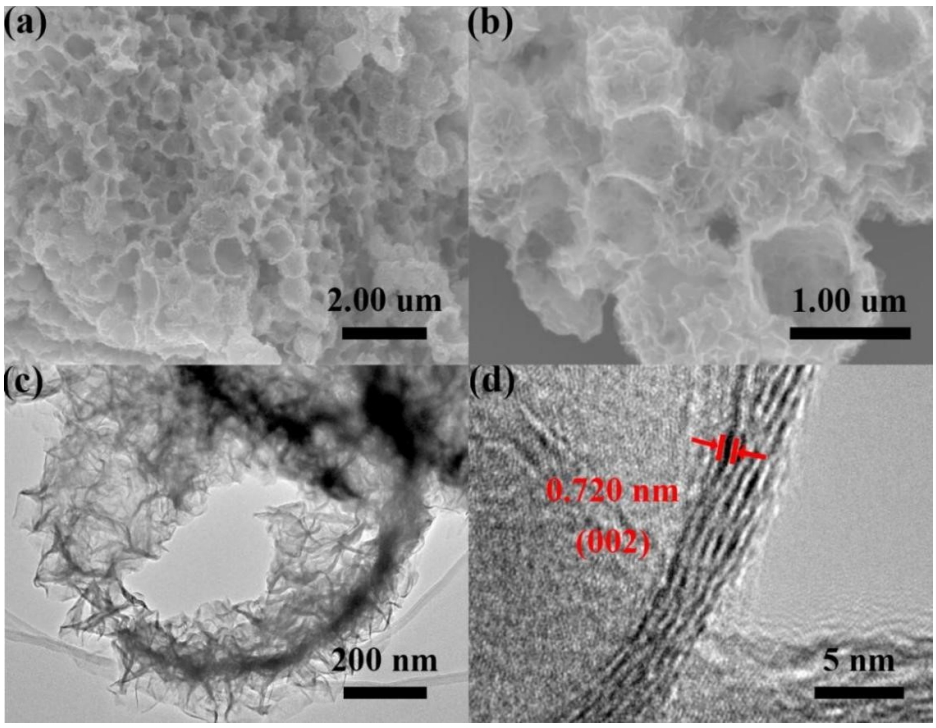

Fig. S8 (a,b) SEM, (c) TEM, and (d) HRTEM images of EH-MoS_2-10.

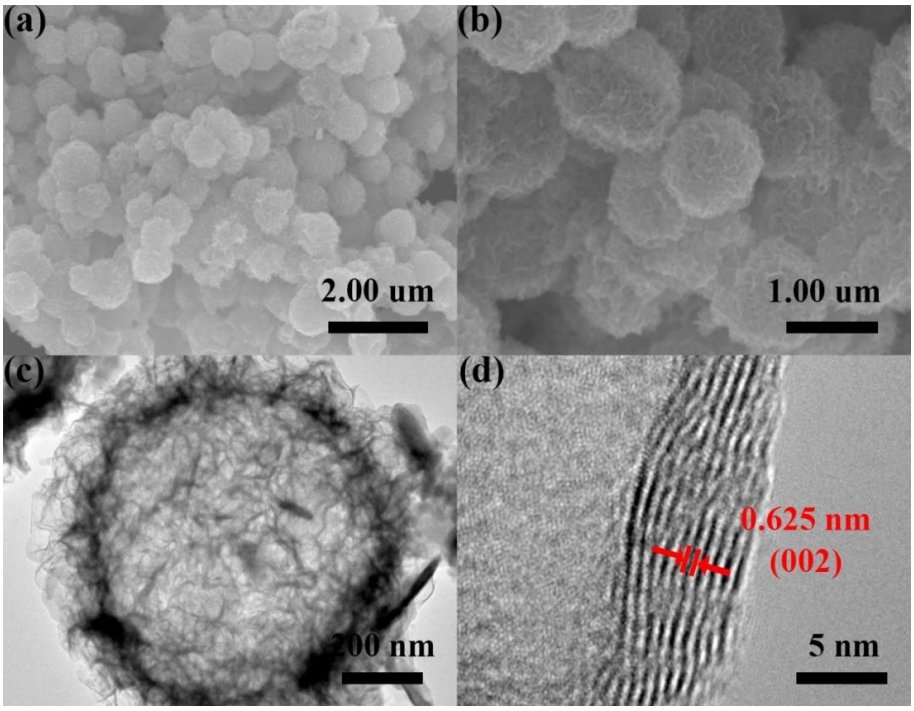

Fig. S9 (a,b) SEM, (c) TEM, and (d) HRTEM images of FH-MoS_2.

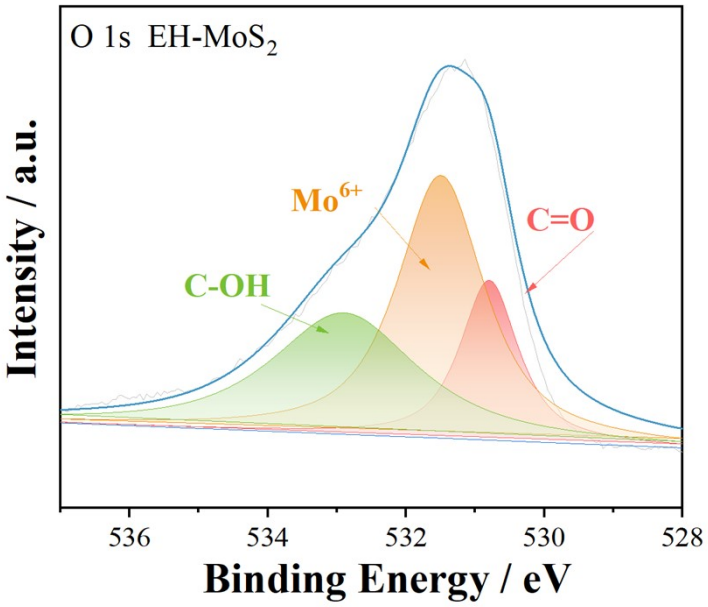

Fig. S10 XPS spectrum of O 1s of EH-MoS_2.

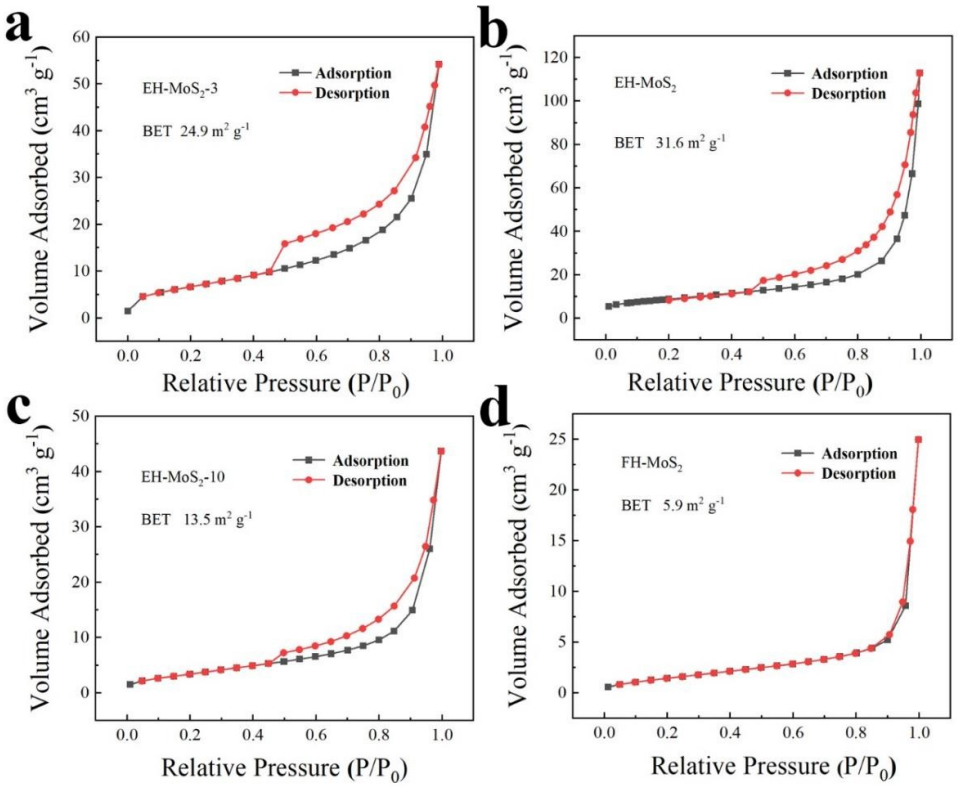

Fig. S11 Nitrogen adsorption and desorption isotherms of (a) EH-MoS_2-3, (b) EH-MoS_2, (c) EH-MoS_2-10, and (d) FH-MoS_2.

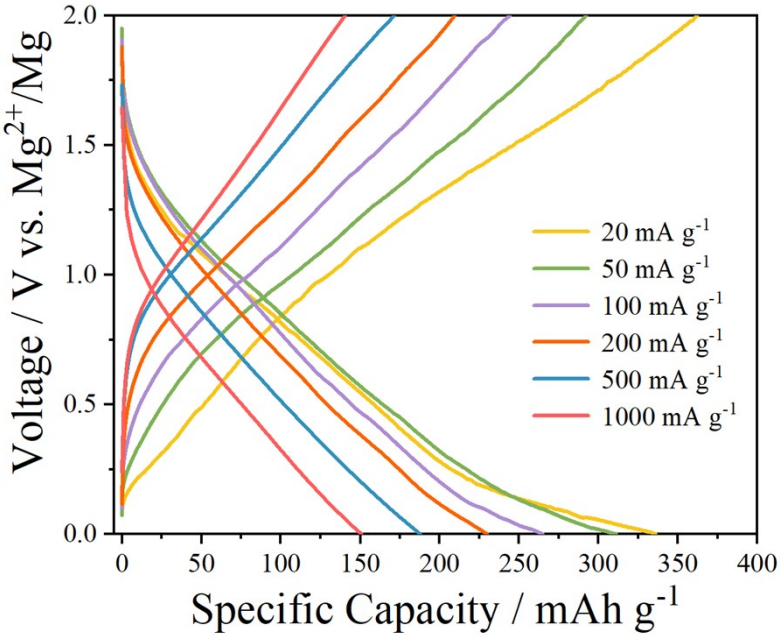

Fig. S12 Galvanostatic charge/discharge curves of EH-MoS_2 at different current densities.

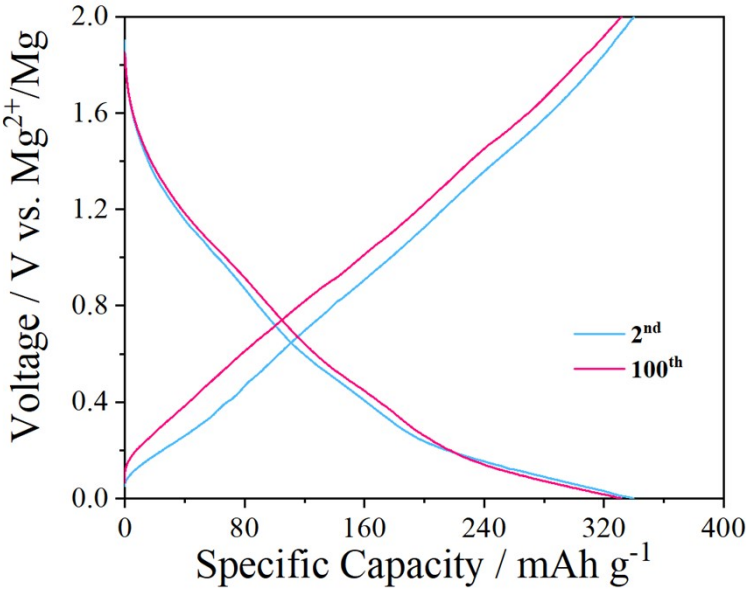

Fig. S13 Galvanostatic charge/discharge curves of EH-MoS_2.

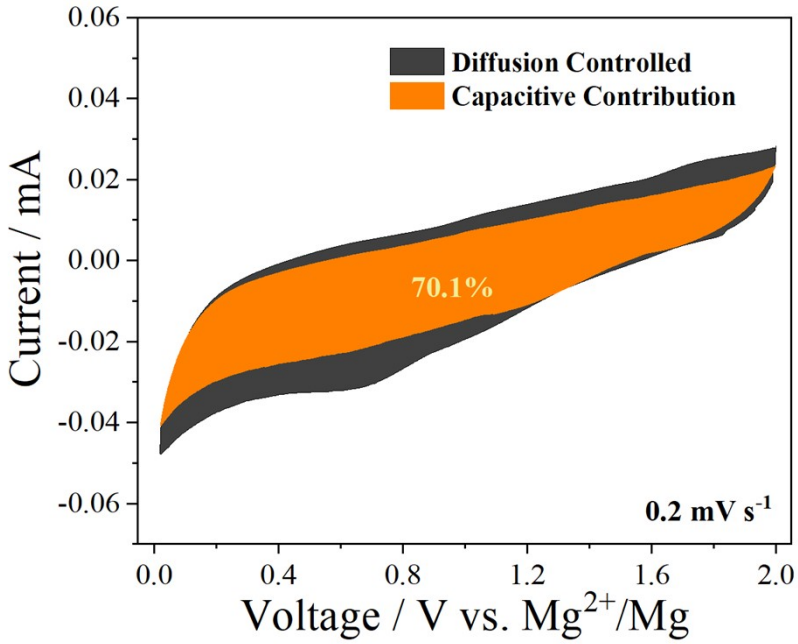

Fig. S14 The capacitive and diffusion-controlled contributions of EH-MoS_2 at the scan rate of 0.2 mV s^{-1}.

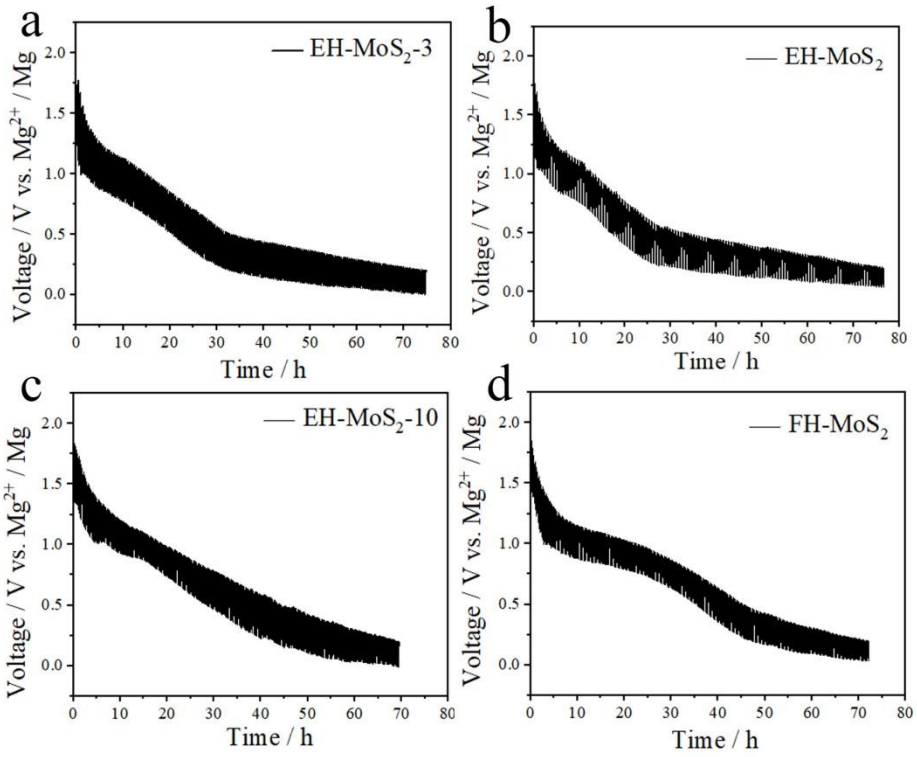

Fig. S15 (a-d) GITT profiles of the discharge process of EH-MoS_2-3, EH-MoS_2, EH-MoS_2-10, and FH-MoS_2.

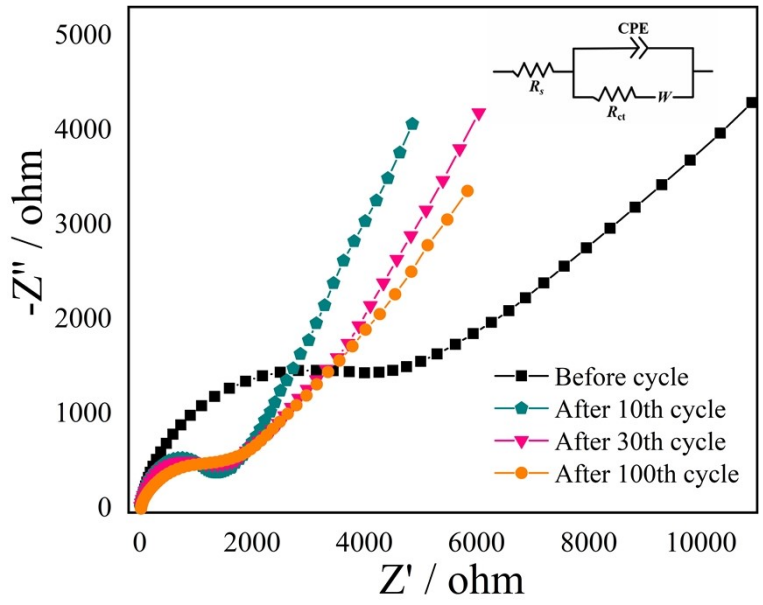

Fig. S16 Nyquist plots and the corresponding equivalent circuit diagram of EH-MoS_2 after different cycles.

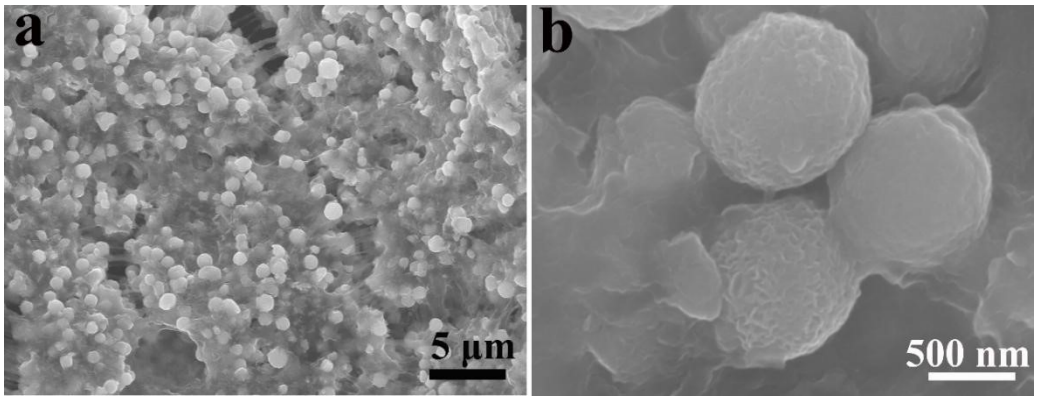

Fig. S17 (a,b) SEM images of EH-MoS_2 after 200 cycles charge–discharge process.

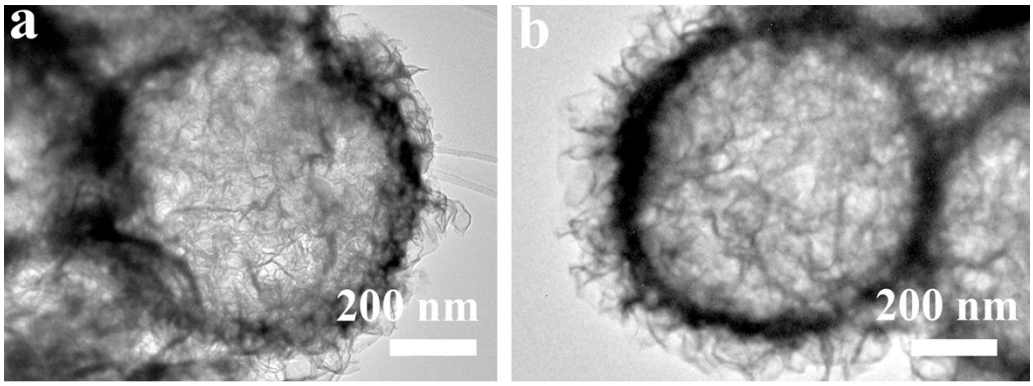

Fig. S18 TEM images of EH-MoS_2 after (a) fully charged and (b) fully discharged states.

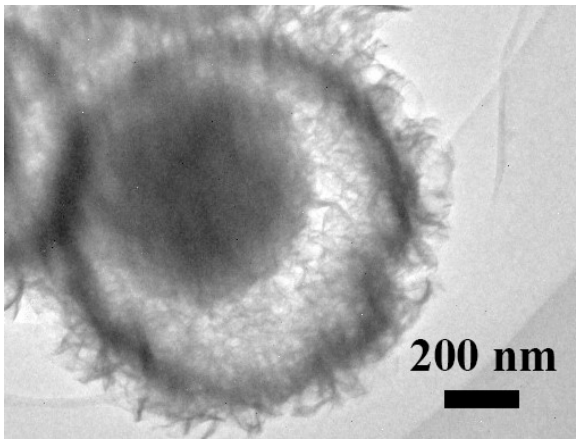

Fig. S19 TEM image of EH-MoS_2-3 after fully charged state.

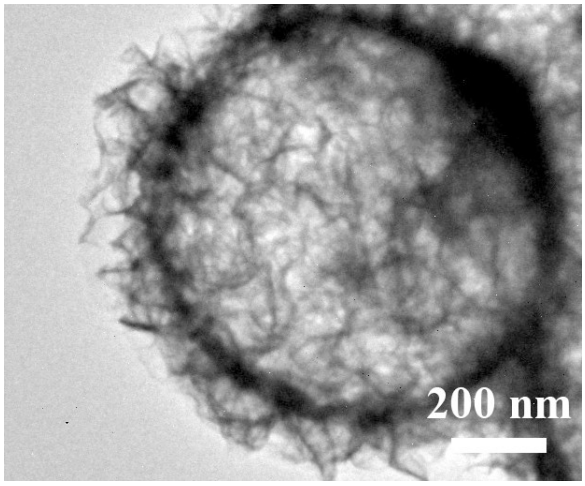

Fig. S20 TEM image of FH-MoS_2 after fully charged state.

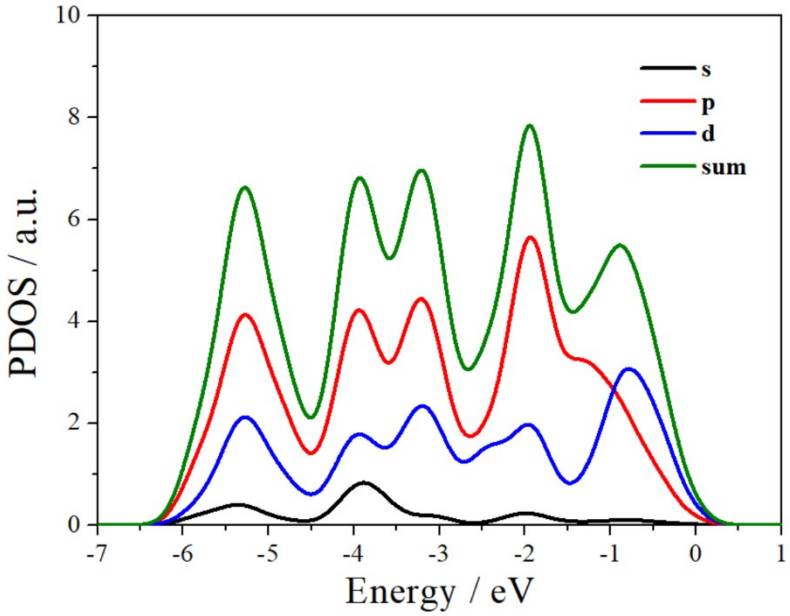

Fig. S21 DOS of EH-MoS_2.

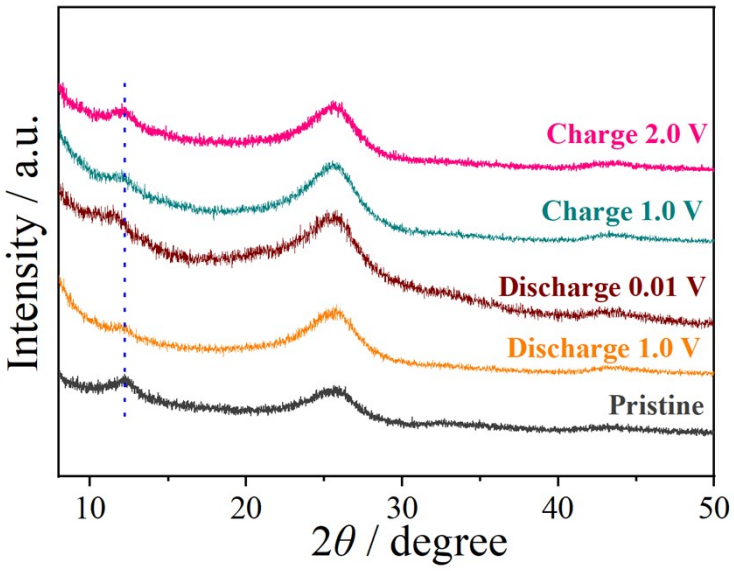

Fig. S22 *Ex situ* XRD patterns of EH-MoS_2 at different voltage test during charge–discharge processes

Table S1. Comparison of electrochemical performance of EH-MoS_2 with other previously reported cathode materials for MIBs.

Electrode material	Current Density (mA g^{-1})	Reversible Capacity (mAh g^{-1})	Cycle Numbers (*n*)	Average Potential of Electrodes (V)	Ref.
EH-MoS_2	20	327.7	200	0.51	This work
	1000	135.9	2000		
$Li_3V_2(PO_4)_3$	100	135	200	0.40	Ref.1
V_2C MXene	50	~110	480	0.38	Ref.2
Cu_2Se	26	~110	30	0.36	Ref.3
Cu_2Se/rGO	26	~65	100		
$LiCrTiO_4$	20	~125	30	0.44	Ref.4
$Ti_3C_2T_x$/CNT	100	~80	500	0.35	Ref.5
$MoSe_2$/C	200	89	100	0.42	Ref.6
V_2MoO_8	20	135	50	0.45	Ref.7
VS_2-GO	90	200	100	0.46	Ref.8
MoS_2 Nano Flowers	1000	107	2300	0.41	Ref.9
MoS_2/G VH	20	260.8	200	0.50	Ref.10
	1000	145.8	2200		
VO_2	20	154.9	100	0.49	Ref.11

References

[1] M. Rashad, H. Zhang, X. Li, H. Zhang, Fast kinetics of Mg^{2+}/Li^{+}hybrid ions in a polyanion $Li_3V_2(PO_4)_3$ cathode in a wide temperature range, *J. Mater. Chem. A* 7 (16) (2019) 9968–9976,

[2] F. Liu, Y. Liu, X. Zhao, K. Liu, H. Yin, L.-Z. Fan, Prelithiated V_2C MXene: A high-performance electrode for hybrid magnesium/lithium-ion batteries by ion cointercalation, *Small* 16 (2020) 1906076,

[3] H. Yuan, N. Wang, Y. NuLi, J. Yang, J. Wang, Hybrid Mg Cu^{2+} /Li^{+} batteries with

Se cathode based on displacement reaction, *Electrochim. Acta* 261 (2018) 503–512,

[4] Y. Yao, L. Zhang, X. Bie, H. Chen, C. Wang, F. Du, G. Chen, Exploration of spinel $LiCrTiO_4$ as cathode material for rechargeable Mg-Li hybrid batteries, *Chem. Eur. J.* 23 (71) (2017) 17935–17939,

[5] A. Byeon, M.-Q. Zhao, C.E. Ren, J. Halim, S. Kota, P. Urbankowski, B. Anasori, M. W. Barsoum, Y. Gogotsi, Two-dimensional titanium carbide MXene as a cathode material for hybrid magnesium/lithium-ion batteries, *ACS Appl. Mater. Interfaces* 9 (5) (2017) 4296–4300,

[6] J.-J. Fan, S.-Y. Shen, Y. Chen, L.-N. Wu, J. Peng, X.-X. Peng, C.-G. Shi, L. Huang, W.-F. Lin, S.-G. Sun, A rechargeable Mg^{2+}/Li^{+} hybrid battery based on sheet-like $MoSe_2$/C nanocomposites cathode. *Electrochem. Commun.* 90 (2018) 16–20,

[7] X. Miao, Z. Chen, N. Wang, Y. Nuli, J. Wang, J. Yang, S. Hirano, Electrospun V_2MoO_8 as a cathode material for rechargeable batteries with Mg metal anode, *Nano Energy* 34 (2017) 26–35,

[8] R. Sun, C. Pei, J. Sheng, D. Wang, L. Wu, S. Liu, Q. An, L. Mai, High-rate and long- life VS_2 cathodes for hybrid magnesium-based battery, *Energy Storage Mater.* 12 (2018) 61–68,

[9] Y. Ju, Y. Meng, Y. Wei, X. Bian, Q. Pang, Y. Gao, F. Du, B. Liu, G. Chen, Li^{+}/Mg^{2+} hybrid-ion batteries with long cycle life and high rate capability employing MoS_2 nanoflowers as the cathode material, *Chem. Eur. J.* 22 (2016) 18073−18079.

[10] X. Yu, G. Zhao, C. Liu, C. Wu, H. Huang, J. He, N. Zhang, A MoS_2 and graphene alternately stacking van der Waals heterostructure for Li^{+}/Mg^{2+} co-intercalation, *Adv. Funct. Mater.* 31 (2021) 2103214.

[11] C. Pei, F. Xiong, J. Sheng, Y. Yin, S. Tan, D. Wang, C. Han, Q. An, L. Mai, VO_2 nanoflakes as the cathode material of hybrid magnesium-lithium-ion batteries with high energy density, *ACS Appl. Mater. Interfaces* 9 (2017) 17060−17066.